THE JOURNAL OF PHYSICAL CHEMISTRY C

Article

pubs.acs.org/JPCC

Atomic Displacive Disorder in $Bi_2Ti_2O_7$

Christopher Turner,*[,†] Paul M. Johns,[†] Evan M. Thatcher,[‡] D. B. Tanner,[‡] and Juan C. Nino[†]

[†]Department of Materials Science and Engineering, and [‡]Department of Physics, University of Florida, Gainesville, Florida 32611, United States

ABSTRACT: The recently synthesized cubic pyrochlore $Bi_2Ti_2O_7$ has been shown to possess displacive disorder in both the anion and cation sublattices. Here, the nature and characteristics of the displacive disorder are further investigated via vibrational spectroscopy. The infrared reflectance was measured over 30−3300 cm^{-1} at temperatures between 20 and 300 K, while the Raman spectra were collected from 50 to 3500 cm^{-1} at room temperature. It is found that $Bi_2Ti_2O_7$ exhibits more than the six modes expected in the Raman spectrum for the ideal pyrochlore structure. In addition, infrared-active modes are also present in the Raman spectra. These two results suggest displacements in the atomic positions of bismuth and oxygen away from their higher symmetry conventional pyrochlore Wyckoff positions and are strong and surprising evidence of disorder at the titanium site. Infrared-active phonon modes have been assigned to specific bending and stretching vibrational modes. The effect of the Bi ion on the O−Bi−O and O′−Bi−O′ phonon modes is discussed.

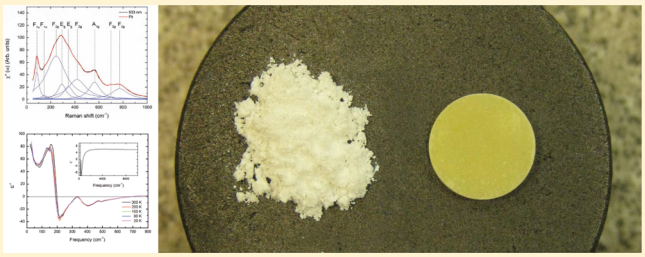

INTRODUCTION

Compounds with the nominal composition $A_2B_2O_7$ containing B_2O_6 octahedral and A_2O' tetrahedral substructures are known as pyrochlores and are assigned to the space group $Fd\bar{3}m$. Bismuth-based pyrochlores have been extensively studied due to their attractive composition-dependent dielectric properties.[1−9] A combination of high permittivity (usually above 100) and low dielectric loss are mainly attributed to their dielectric relaxor behavior, where the real and imaginary parts of the relative permittivity are both frequency- and temperature-dependent.

Recently, the synthesis and densification of $Bi_2Ti_2O_7$ was achieved via coprecipitation and microwave sintering.[10] The availability of sintered bismuth titanate pyrochlore specimens finally allows the study of both the physical and chemical properties of the compound in the bulk.

Toward the understanding of the crystal structure−dielectric property relationships in $Bi_2Ti_2O_7$, it is important to recall that in the ideal pyrochlore structure ($A_2B_2O_7$, space group 227, origin 1), the A cation resides at the 16*c* site, the B cation at the 16*d* site, O at the 48*f* site, and the seventh oxygen, typically denoted as O′, at the 8*a* position. However, density-functional theory (DFT) calculations by Esquivel-Elizondo et al.[10] indicate that the atoms within the $Bi_2Ti_2O_7$ crystal do not reside at the ideal pyrochlore positions. Rather, in $Bi_2Ti_2O_7$, the A cation (bismuth) is not located in its ideal 16*c* (0, 0, 0) but is in the 96*g* (0.015, 0.015, 0.964) site to accommodate the Bi lone pair electron.[11] High-resolution XRD and neutron diffraction data have confirmed this predicted Bi displacement in $Bi_2Ti_2O_7$.[12] The O′ atom is also not in the ideal pyrochlore position: instead of residing in the 8*a* site (1/8, 1/8, 1/8), it is displaced to the 48*f* (*x*, 1/8, 1/8) position. As a result of these displacements, it is expected that $Bi_2Ti_2O_7$ will stray from the traditional group theory rules for a stable pyrochlore structure.

In addition to the Bi and O′ displacement, a noteworthy feature of the theoretical (DFT) study is a large isotropic thermal parameter ascribed to the Ti cation in the 16*d* position.[10] This was reported to be the result of the displacement of the bismuth atom toward the 96*g* site which in turn causes a separation between the regularly symmetric Bi and O atoms, thus resulting in an undercoordinated Ti atom. In an effort to satisfy this O undercoordination, the Ti cation is predicted by DFT simulations to displace to the 96*g* position. However, it is important to recognize that DFT simulations do not take into account thermal considerations (since simulations are performed at 0 K) and that experimental diffraction to date has not yielded evidence of Ti shifting from the 16*d* position to the 96*g*. Therefore, in the past, a large thermal isotropic parameter has been ascribed to the Ti cation instead of reporting a displacement toward 96*g* positions.

The proposed atomic displacements of the Bi and O′ atoms in $Bi_2Ti_2O_7$ are similar to that observed in another bismuth pyrochlore, $Bi_{1.5}Zn_{0.92}Nb_{1.5}O_{6.92}$ (BZN).[4,11,13] Nonetheless, what is striking is that this displacement would occur without atomic substitutional atoms (e.g., Bi and Zn in the A-site) and multiple site occupancy (e.g., Zn in both A- and B-sites, both of which are always present in BZN and related Bi pyrochlores.

To understand further the implication of the displacements on the local atomic structure and phonons, Table 1 displays the factor group analysis for $Bi_2Ti_2O_7$ following the DFT positions by Esquivel-Elizondo et al.[10] The irreproducible representation

Received: September 22, 2014
Revised: November 5, 2014
Published: November 11, 2014

   dx.doi.org/10.1021/jp5095883 | J. Phys. Chem. C 2014, 118, 28797−28803

Table 1. Optical Modes of $Bi_2Ti_2O_7$[a]

O_h^7	modes				acoustic modes	optical modes	selection rules
	Bi	Ti	O	O′			
	C_s	D_{3d}	C_{2v}	C_{2v}			
	96*g*	16*d*	48*f*	48*f*			
A_{1g}	2	0	1	1	0	4	**Raman**
A_{1u}	1	0	0	0	0	1	silent
A_{2g}	1	0	0	0	0	1	silent
A_{2u}	2	1	1	1	0	5	silent
E_u	3	1	1	1	0	6	silent
E_g	3	0	1	1	0	5	**Raman**
F_{1g}	4	0	2	2	0	8	silent
F_{2g}	5	0	3	3	0	11	**Raman**
F_{1u}	5	2	3	3	1	12	**infrared**
F_{2u}	4	1	2	2	0	9	silent

[a] $\mathbf{4A_{1g}(R)} + A_{2g}(-) + A_u(-) + 5A_{2u}(-) + 6E_u(-) + \mathbf{5E_g(R)} + 8F_{1g}(-) + \mathbf{12F_{1u}(IR)} + \mathbf{11F_{2g}(R)} + 9F_{2u}(-)$.

(Γ) was derived using the normal mode determination tables.[14] Using Schönflies notation, the space group for $Bi_2Ti_2O_7$ is O_h^7; bismuth has a C_s point group symmetry representing a cyclic point group with a twofold rotation, while titanium has a dihedral D_{3d} point group symmetry with a threefold rotation and three twofold axes perpendicular to the threefold axis and a horizontal mirror plane. Both O and O′ are represented by the point group symmetry C_{2v} which is a cyclic group with a twofold rotation and two vertical planes.

In the $Bi_2Ti_2O_7$ structure the anticipated modes, following normal coordinate analysis methods, are

$$\mathbf{4A_{1g}(R)} + A_u + A_{2g} + 5A_{2u} + 6E_u + \mathbf{5E_g(R)} + 8F_{1g} + \mathbf{12F_{1u}(IR)} + \mathbf{11F_{2g}(R)} + 9F_{2u} \quad (1)$$

In both Table 1 and eq 1, the acoustic mode has been subtracted from the total number of vibrational modes. Furthermore, it has also been proposed by Chen et al.[15] that disorder in the A site leads to a break in the selection rules, and therefore, the normally IR-active low-frequency modes, such as F_{1u}, may also appear in the Raman spectra.

Atomic (valence) force field analysis allows for the identification of the type of interactions that contribute to each phonon mode. It also provides an insight into the structure of a cell by comparison with similar crystals, such that atomic disorder can be discerned. This has been previously demonstrated for pyrochlores by Vandenborre et al.[16] and applied to perform a detailed comparison across a series of titanate and stannate pyrochlores.

Based on this, in the present article, we utilize Raman and IR spectroscopy techniques to gain insight into the nature and characteristics of the local structure of $Bi_2Ti_2O_7$ and corroborate prior crystallographic and computational studies on the crystal structure of the compound in particular as it relates to its atomic displacive disorder.[17]

EXPERIMENTAL SECTION

Pyrochlore $Bi_2Ti_2O_7$ ceramic pellets were created via the coprecipitation chemical synthesis technique, following the procedure described in detail in our previous work.[10] Raman spectroscopy was performed on phase-pure calcined powder as well as sintered pellets of 10 mm diameter and 1.5 mm height. The phase purity of the samples was verified by XRD, and the obtained density was greater than 95%.

The presented Raman measurements were performed on a Thermo Scientific DXR Raman microscope system. The Raman shift was measured from 50 to 3500 cm^{-1} by exciting the sample with a 532 nm photon beam from a 1 mW laser. The spectrometer was equipped with a 900 line/mm filter grating and a 50 μm spectrograph aperture. The measurement data was compiled over 10 exposures with 512 background exposures, each taken at room temperature with an exposure time of 2 s. Complementary measurements were taken on a Horiba MicroRaman system with a 532 nm laser.

Temperature-dependent reflectivity was obtained using a Fourier transform spectrometer (Bruker IFS 113v) in conjunction with a liquid helium cooled Si bolometer (over 30−700 cm^{-1}) and a room temperature DTGS detector (over 650−3300 cm^{-1}). The reflection stage provided an angle of incidence of 8° for the light. Temperatures between 20 and 300 K were obtained in a Hanson flow cryostat with polyethylene (far-infrared) or KBr windows (mid-infrared). Room temperature data between 3000 and 37 000 cm^{-1} were taken using a Zeiss microscope photometer.

In order to combine the different spectra, a suitable region of overlap was chosen where the spectra were in agreement. An integral was taken to find the area under the curve of each spectra within this region. The higher frequency spectrum was then multiplied by the ratio of these areas such that the areas became equal. A weighted average was then taken beginning at the low-frequency edge of the selected region with all of the weight given to the lower frequency spectrum and ending at the high-frequency edge with all of the weight given to the higher frequency spectrum.

RESULTS AND DISCUSSION

As mentioned in the Introduction, it is anticipated that $Bi_2Ti_2O_7$ will exhibit 20 Raman-active (R) modes, 12 infrared-active (IR) modes, and one F_{1u} acoustic mode.

Raman Spectroscopy. As discussed at length by Esquivel-Elizondo et al.,[10] $Bi_2Ti_2O_7$ can be considered a metastable compound, with dissociation into $Bi_4Ti_3O_{12}$ and $Bi_2Ti_4O_{11}$ commonly occurring. This crystal chemistry had previously prevented the synthesis of $Bi_2Ti_2O_7$ sintered ceramics until fast firing techniques like microwave sintering were used. Because Raman spectroscopy provides the capability to measure the spectra of samples that are sintered solids, powders, or even particulates suspended in a fluid, it is an excellent tool for characterizing whether a material undergoes a structural transformation when sintered or processed. Therefore, spectra of $Bi_2Ti_2O_7$ were taken in both powder and solid pellet form. These spectra, shown in Figure 1, were identical for the powder and pellet samples, further confirming that sintering of $Bi_2Ti_2O_7$ powder does not induce a structural change, in agreement with X-ray diffraction results.[10] This lends further evidence in favor of the modified phase diagram,[10] which establishes the appearance of the pyrochlore phase in the Bi_2O_3−TiO_2 system.

The $Bi_2Ti_2O_7$ Raman spectrum was analyzed by solving for the imaginary part of the Raman susceptibility in order to observe and fit the individual vibrational modes. This was accomplished through the transformation of the measured data to find the imaginary part of the Raman susceptibility, $\chi''(\omega)$.[18] The susceptibility is a function of the Raman scattering cross section and the Bose scattering factor. This was resolved by

dx.doi.org/10.1021/jp5095883 | J. Phys. Chem. C 2014, 118, 28797−28803

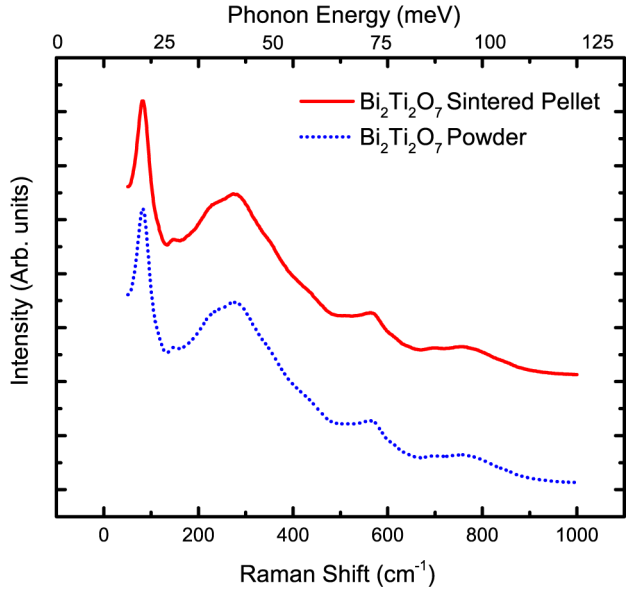

Figure 1. Room temperature Raman spectra of $Bi_2Ti_2O_7$ powder and sintered pellet.

treating the collected data with the Bose–Einstein distribution, $\eta(\omega)$.

$$\eta(\omega) = \frac{1}{e^{\hbar\omega/k_bT} - 1} \tag{2}$$

The transformed Raman susceptibility was modeled using a sum of Lorentzian functions used to assign the Raman modes, as shown in Figure 2.

$$\chi''(\omega) = \sum_j^n \frac{A_j}{1 + \frac{4(\omega - \omega_{0j})^2}{\gamma_j^2}} \tag{3}$$

where each fitted peak is characterized by a center frequency ω_0, a local maximum A_j, and a width γ_j. Table 2 shows parameters obtained from the Lorentzian fitting. The $Bi_2Ti_2O_7$ modes were assigned by comparing to typical bismuth and

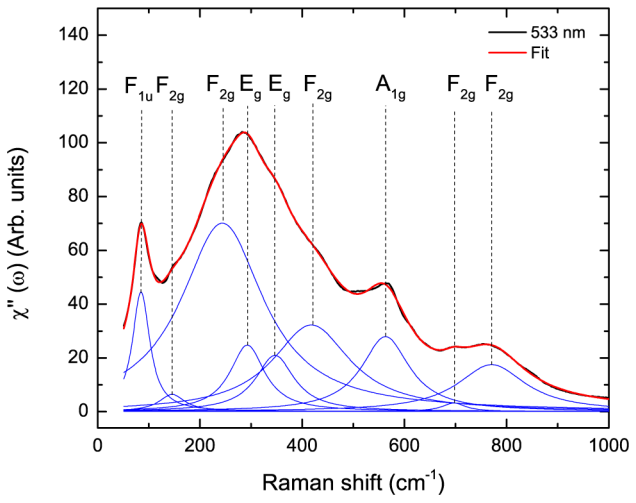

Figure 2. Raman spectra transformed by the Bose–Einstein factor. The obtained imaginary part of the Raman susceptibility was fitted to a sum of Lorentzian functions. The figure shows the data (black), the fit (red), and the individual contributions to the fit (blue).

titanate pyrochlores[18−20] as shown in Table 2, but with the addition of normally infrared active F_{1u} modes as explained below. Because the area of each fitted mode is an arbitrary value (hence the representation by integrated intensity), the error presented is the calculated standard error of each mode represented as the fraction of each peak's total area.

Through the automated Lorentzian fit algorithm, nine optically active Raman vibrational modes were identified. These nine peaks each represent an interaction (bend or stretch) in the bonds between oxygen atoms and Bi or Ti atoms. The Raman-mode properties are a function of the valence force field emitted by each atom and each corresponding bond's interaction with the Raman photon.

While each peak is assigned to a main phonon mode in Figure 2 and Table 2, it is also true that when one bond is set into vibration, this motion has an effect on the rest of the lattice; i.e., when a bending occurs between one bond species, the other atomic bonds in the structure will bend and stretch in reaction. This combined set of phonon motions has been clearly shown for the pyrochlore structure, by Vandenborre et al.[20] It has been observed that platinates and stannates display sharp peaks in the spectra, much more than the zirconates, hafnates, and titanates. This difference is explained by a greater deviation from ideal pyrochlore symmetry (D_{3d}) in the latter compounds.[21] As such, materials with high displacive disorder will typically exhibit broader peaks within the Raman spectra. Therefore, here we propose that the relative broadening of the Raman peaks observed is the result of the atomic position displacement causing local asymmetry within the crystal that produces a stronger force field reaction from a single phonon interaction.

In previous studies of pyrochlore titanates,[16] valence force field constants for stretch, bend, and combination bend–stretch interactions have been calculated for a variety of compounds. The potential energy of each mode is dependent on the sum of the strength of each contributing interaction, namely how the strength of the valence force and the incoming photon cause a series of singular or multiple elastic interaction throughout the lattice. Low-frequency Raman modes found in pyrochlores are generally found to be a combination of several bends and stretches, as photon interactions on the lattice due to single bends/stretches induce elastic effects at other sites. Calculation of individual interaction valence force fields in $Bi_2Ti_2O_7$ is beyond the scope of this work; however, based on the trends observed in other pyrochlores, we postulate that modes fitted to large and wide Lorentzian indicate that the interaction causing the vibration arises from a combination of several motions, each contributing an additional amount of energy into the vibration. For example, the F_{2g} mode centered at 244 cm^{-1} has a width of 197 cm^{-1} which is attributed to the combination of the Bi–O stretch and the O–Bi–O′ bend motions. Likewise, sharper peaks indicate that a vibrational mode is likely influenced by a single interaction.

It is important to note that previous work on the theoretical $Bi_2Ti_2O_7$ structure and vibrational spectra was performed by Patterson through DFT.[23] The DFT simulations performed by Patterson were performed for $Bi_2Ti_2O_7$ in both the $Pna2_1$ and $Fd\bar{3}m$ crystal structures. However, both structural studies and the data presented in this paper confirm that $Bi_2Ti_2O_7$ has a cubic $Fd\bar{3}m$ structure. Although the Bi ion displacement was included in these DFT calculations, the theoretical Raman spectra did not predict the Raman active F_{1u} modes observed in this work.

dx.doi.org/10.1021/jp5095883 | J. Phys. Chem. C 2014, 118, 28797−28803

Table 2. Parameters for $Bi_2Ti_2O_7$ in the Lorentzian Fitting of the Raman Spectra

integrated intensity (arb. unit)	ω_{0j} (cm^{-1})	γ_j (cm^{-1})	assignment	type	error (%)
13	85	41	F_{1u}	O−Bi−O bend and O−Bi−O′ bend	2
3	146	62	F_{2g}	Bi−O stretch and O−Bi−O′ bend	15
100	244	197	F_{2g}		6
15	293	83	E_g	3*Ti−O stretch	20
14	347	92	E_g		2
43	418	185	F_{2g}		17
23	563	114	A_{1g}	O−Ti−O bend	3
1	697	55	F_{2g}	2*Ti−O stretch	8
21	771	163	F_{2g}		17

Table 3. Observed Raman Vibrational Mode Frequencies of Bismuth and Titanate Pyrochlores

			F_{2g}/E_g		F_{2g}	A_{1g}	F_{2g}	F_{2g}
$Y_2Ti_2O_7$[16]	225	–	318	333	–	527	531	586
$Gd_2Ti_2O_7$[25]	205	260	310	325	450	517	554	677
$Dy_2Ti_2O_7$[25]	212	269	308	328	451	519	550	693
$Ho_2Ti_2O_7$[25]	214	297	311	329	452	522	562	701
$Lu_2Ti_2O_7$[26]	188	–	313	336	458	520	609	712
exptl $Bi_2Ti_2O_7$	146	244	293	347	418	563	697	771
theor. $Bi_2Ti_2O_7$[23]	–	262	281	–	395	535	537	711
$Bi_{3/2}MgNb_{3/2}O_7$[18]	–	230	346	–	419	511	599	786
$Bi_{3/2}MgNb_{3/2}O_7$[18]	–	216	297	–	430	529	620	758
$Bi_{3/2}Zn_{0.92}Nb_{3/2}O_{6.92}$[18]	–	256	342	–	420	526	610	766
$Bi_{3/2}ZnTa_{3/2}O_7$[18]	–	208	281	–	434	540	624	744

To reconcile this, it is worth mentioning that, in general, pyrochlores have their A−O atom interactions dominant at low frequencies and their B−O atom interactions prevalent at high frequencies. The low-frequency range of the Raman spectrum (from 70 to 180 cm^{-1}) has been proposed to be composed of typically IR-active F_{1u} vibrational modes due to the displacive disorder of the A-site observed in Bi pyrochlores.[18] In a study of Sm, Gd, Yb, and Y titanate pyrochlores by Vandenborre,[19] Raman spectra comparison of low-frequency modes were determined to not be fundamental frequencies and were attributed to TiO_6 octahedra distortion and/or displacement in the A-site cation. The F_{1u} modes activated primarily due to the O−A−O and O−A−O′ bending, assigned at 85 and 145 cm^{-1}, similarly occur in the Raman spectra of $Bi_2Ti_2O_7$ due to the displacement of the Bi atom from a high-symmetry position in the crystal lattice.[18]

As stated before, the Bi atom in $Bi_2Ti_2O_7$ differs from the ideal pyrochlore structure by occupying the 96*g* Wyckoff position instead of the 16*c*. This displacive disorder in $Bi_2Ti_2O_7$ further supports the idea proposed by Arenas et al.[18] of a relaxation in the selection rules allowing for the F_{1u} mode to be seen in the Raman spectra.

Following this, the 180−500 cm^{-1} bands are composed of F_{2g} and E_g modes.[18] The first F_{2g} mode is generally assigned between 200 and 240 cm^{-1} for titanates,[19] and in the case of $Bi_2Ti_2O_7$ the lowest F_{2g} is assigned to the mode observed at 146 cm^{-1}. This vibrational mode is attributed to a combination of a stretching interaction between the Bi−O bonds, which induces an additional bending in the O−Bi−O′ bond. The E_g modes assigned to 294 and 347 cm^{-1} and the F_{2g} mode assigned at 419 cm^{-1} are principally due to a stretching of the Ti−O bond which causes a reaction from other O−Ti−O bonds.

The higher frequencies consist of A_{1g} and F_{2g} vibrational modes, which are purely due to the Ti−O modes.[20] The lower A_{1g} mode, assigned at 564 cm^{-1}, is due to O−Ti−O bond bending. The two highest modes at 697 and 771 cm^{-1} are at frequencies that are usually ascribed as combination bands or overtones. However, studies into other displaced pyrochlores have shown these modes to be related to a B site and oxygen stretch.[18,24] These two bands are designated as F_{2g} at 697 and 771 cm^{-1} and are due to the stretching of the Ti−O bond. In a recent Raman study on the behavior of ^{18}O-enriched $Lu_2Ti_2O_7$ and $Dy_2Ti_2O_7$ pyrochlores,[22] low-frequency phonons were ascribed to Ti^{4+} vibrations without the involvement of oxygen vibrations. However, support for this argument comes from the positioning of rare earth (A site) and Ti ions at the centers of inversion symmetry; this does not likely apply toward $Bi_2Ti_2O_7$ with the observation of Bi displacement. Moreover, the large difference in ionic radii between Bi and Dy or Lu results in vastly different anionic and cationic coordination environments. Therefore, it is unlikely that a similar Ti-vibration phonon is present in $Bi_2Ti_2O_7$.

Table 3 presents the vibrational modes of several pyrochlore titanates with their corresponding frequencies. The $Bi_2Ti_2O_7$ Raman modes follow the general behavior of the titanate pyrochlores up until the 500 cm^{-1} range, at which point the A_{1g} and F_{2g} modes are observed at notably higher frequencies, in disagreement with the theoretically calculated modes.[23] This can be explained by a possible disorder in the titanium position in the $Bi_2Ti_2O_7$ crystal structure, which would affect the Ti−O bond interactions, and accordingly the A_{1g} and F_{2g} modes. Recalling the large isotropic parameter assigned to the Ti atom, the observed Raman spectra provide additional evidence suggesting that the Ti atom may in fact be displaced,[10] which would in turn affect Raman interactions.

Infrared Spectroscopy. *Reflectance Spectra.* The temperature dependent reflectance of a sintered $Bi_2Ti_2O_7$ pellet over 30 and 37000 cm^{-1} is shown in Figure 3. The high reflectance value seen at low frequencies is consistent with the large static permittivity values of $Bi_2Ti_2O_7$ (see Discussion below.) As

dx.doi.org/10.1021/jp5095883 | J. Phys. Chem. C 2014, 118, 28797−28803

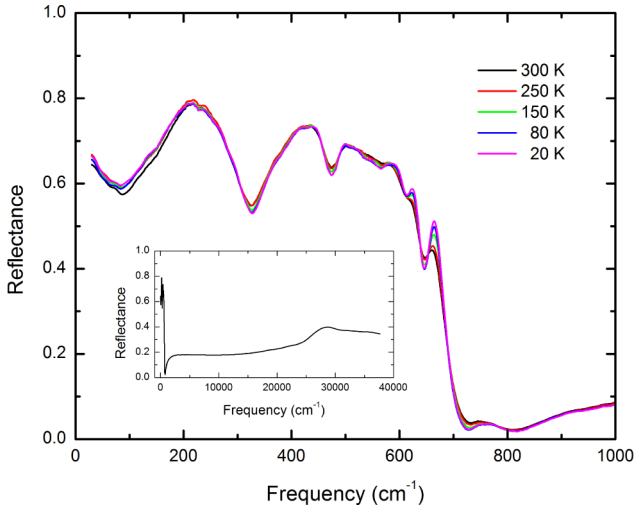

Figure 3. Reflectance of $Bi_2Ti_2O_7$ at temperatures between 20 and 300 K.

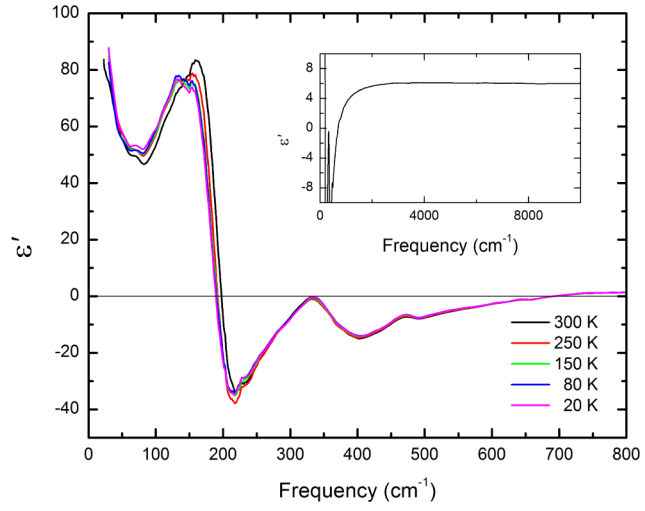

Figure 4. Real part of the dielectric function (ε') of $Bi_2Ti_2O_7$ at temperatures between 20 and 300 K.

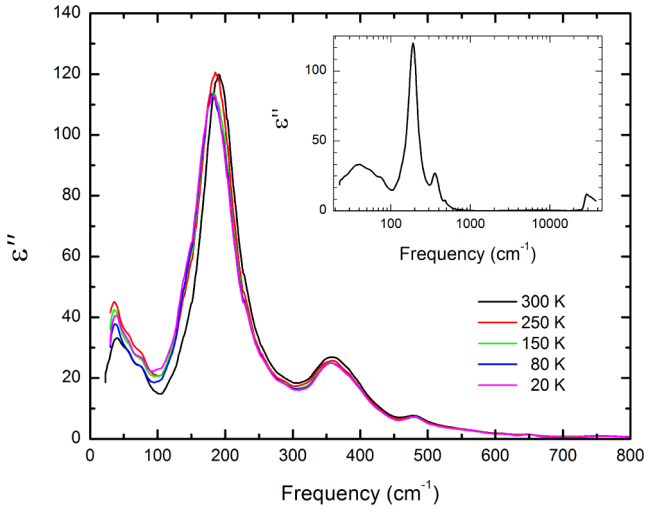

Figure 5. Imaginary part of the dielectric function (ε'') of $Bi_2Ti_2O_7$ at temperatures between 20 and 300 K.

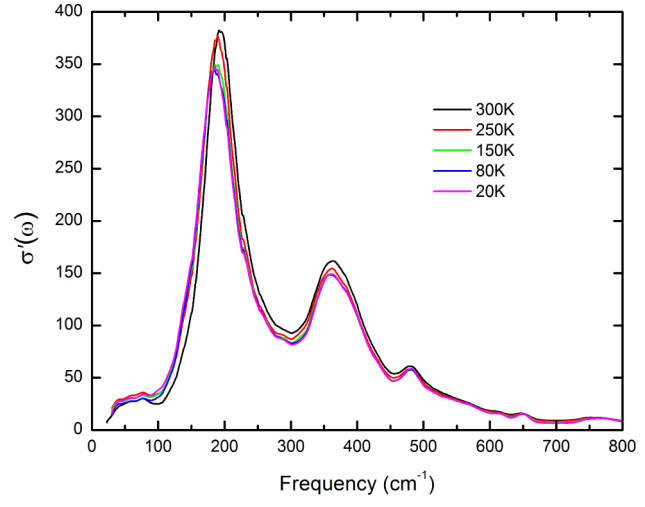

Figure 6. Real part of the optical conductivity (σ') of $Bi_2Ti_2O_7$ at temperatures between 20 and 300 K.

temperature changes, the spectra change only slightly, with a few percent increase at lower temperatures. We conclude that there is no phase transition present in this temperature range.

Kramers–Kronig Analysis. The frequency-dependent phase shift upon reflection can be calculated from the measured single bounce reflectivity via the Kramers–Kronig integral.[27] The high-frequency behavior of $Bi_2Ti_2O_7$ from 80 000 to 242 000 000 cm^{-1} (10–30 000 eV) is determined using scattering functions from Henke[28] and is based on the density and cubic structure of the pyrochlore. The behavior above this range is taken to follow free electron behavior, $R \approx \omega^{-4}$. The gap between the 37 000 cm^{-1} end to the measured reflectance and the start of the calculated X-ray data is bridged with a power law to the third degree in $1/\omega$. The low frequency extrapolation, covering 0–30 cm^{-1}, uses the reflectance calculated from the oscillator model fit described in the next section. With the phase shift calculated from measured data using Kramers–Kronig methods, other optical constants, including the real and imaginary parts of the dielectric constant (Figures 4 and 5) and the optical conductivity (Figure 6), can be easily found.[27]

We note that the optical conductivity and permittivity plots show the widths of the phonons to be quite substantial. This, however, is not in disagreement with Chen et al., who also found broad phonon spectra in bismuth-based pyrochlores.[15] We can also see from the real part of the permittivity that there is a weakening of the mode at 160 cm^{-1} with decreasing temperature. There is a corresponding softening of this peak in Figures 5 and 6. The interband electronic contribution to the optical conductivity can be clearly seen in the inset of Figure 5.

Oscillator-Model Analysis. To complement the Kramers–Kronig analysis and in order to assign the contribution to the permittivity from each mode, oscillator model fits were conducted on the measured reflectance. Oscillator fits of the experimental measurements are obtained by the dispersion analysis (DA) method, which solves for each oscillator based on its strength, width, and frequency. The DA method requires the crystal's reflectivity to be in agreement with the oscillators. To solve for the reflectance the Fresnel formula is employed

$$R(\omega) = \frac{(n-1)^2 + k^2}{(n+1)^2 + k^2} \quad (4)$$

dx.doi.org/10.1021/jp5095883 | J. Phys. Chem. C 2014, 118, 28797–28803

with R(ω) the reflectance, n the refractive index, and k the extinction coefficient of the material. In turn, n and k are related to the dielectric function ε via

$$n + ik = \sqrt{\varepsilon' + \varepsilon''} \tag{5}$$

with ε' and ε'' the real and imaginary parts of the dielectric function

$$\varepsilon' = n^2 - k^2 = \varepsilon_\infty + \sum_j \frac{4\pi\rho_j\omega_j^2(\omega_j^2 - \omega^2)}{(\omega_j^2 - \omega^2)^2 + (\gamma_j\omega)^2} \tag{6}$$

$$\varepsilon'' = 2nk = \sum_j \frac{4\pi\rho_j\omega_j^2(\gamma_j\omega)}{(\omega_j^2 - \omega^2)^2 + (\gamma_j\omega)^2} \tag{7}$$

Each oscillator is described by its strength ρ_j, width γ_j, and frequency ω_j.

As previously discussed, a factor group analysis that uses the displaced coordinates (albeit without Ti displacement, shown in Table 1) yields a total of 12 allowable IR active modes. Here, 13 oscillators are required to fit the infrared reflectivity spectra for $Bi_2Ti_2O_7$. The parameters for these oscillators are presented in Table 4. The longitudinal optic (LO) modes occur at the zeros of the undamped dielectric function. We estimate the LO mode frequencies here by temporarily setting the damping of the fit to 0.1 cm^{-1} and observing the zero crossings of the real part of the permittivity.

Table 4. Parameters for the Phonon Modes in the 20 K Infrared Spectrum of $Bi_2Ti_2O_7$

$Bi_2Ti_2O_7$			20 K		
mode	mode assignment	resonant frequency ω (cm^{-1})	oscillator strength $\Delta\varepsilon$	damping coefficient γ (cm^{-1})	LO mode ω (cm^{-1})
ω_7[a,c]	(O′−A−O′) bend	≈10	–	–	
ω_7[a]	(O′−A−O′) bend	39	20.6	27	44
ω_7[a]	(O′−A−O′) bend	56	4.70	24	59
ω_7	(O′−A−O″) bend	77	4.81	35	80
ω_6	(O−A−O) bend	186	42.9	68	265
ω_5	(A−BO_6) stretch	273	1.40	77	319
ω_4[a]	(O−B−O) bend	357	3.05	58	386
ω_4	(O−B−O) bend	398	1.36	57	474
ω_3	(A−O) stretch	483	0.365	41	528
ω_2	(A−O′) stretch	532	0.103	43	566
ω_1[a]	(B−O) stretch	569	0.0653	38	612
ω_1[a]	(B−O) stretch	613	0.0123	18	647
ω_1	(B−O) stretch	650	0.0147	12	700
ω_n[b]		764	0.0301	35	774
ε_∞			3.05		
ε_{sum}			85.3		

[a]Mode splitting. [b]Split A−O′ mode. [c]Modes that are observed but not included in the fit as described in present work.

The low-frequency section of the ε'' and σ' plots above suggests the presence of a mode below 30 cm^{-1}. Without this mode, the static dielectric constant, obtained by summing the lattice and electronic contributions from the fit, is ≈85, lower than the dielectric constant of ref 10, ε_{sum} = 115. The additional low-frequency mode may account for this difference.

Because of the large mass of Bi, the resonance frequencies of low-frequency oscillators in conventional pyrochlores are pushed down to even lower frequency values. A comparison of titanate pyrochlores performed by Kumar et al. shows the trend of decreasing low-frequency oscillators as the mass of the A site atom increases.[29] Bismuth is the heaviest atom crystallizing a titanate in the pyrochlore structure, and thus the O′−A−O′ bend and O−A−O bend modes are expected to be pushed down to lower frequencies when compared with previously reported pyrochlore titanates. The O−A−O bend mode is observed at 186 cm^{-1} and the O′−A−O′ bending mode is observed at the lower wavenumbers (<77 cm^{-1}) and through extrapolation could possibly be pushed further down near 10 cm^{-1}, which would explain the increase in reflectivity in the low-frequency region. Although outside of the scope of this work, it would be ideal to complement this data with terahertz spectroscopy investigations to further corroborate this interpretation.

Finally, the data show that bismuth titanate exhibits a phonon mode at around 764 cm^{-1}, identified as ω_n^b in Table 4. This feature is also observed in BZN and related pyrochlores has been attributed to disorder of the A site and static displacements of the O′,[15] this A−O′ disorder is also found in $Bi_2Ti_2O_7$.

Taken as a whole, the Raman and IR spectra are strong evidence of displacive disorder of both the A and B site of $Bi_2Ti_2O_7$. Bismuth displacive disorder is shown by the presence of an IR assigned mode in the Raman spectra. The atypical behavior of the Ti−O modes in the higher range of the Raman spectra provides evidence of displacement of the Ti atomic position. The IR spectra further reveals disorder in the A and O′ sites due to the splitting of the appearance of the ω_n^b mode.

CONCLUSION

The Raman spectroscopy of the pyrochlore $Bi_2Ti_2O_7$ was measured on both calcined powder and sintered ceramic, showing that both spectra were identical. This provides evidence that no major structural change occurs during sintering. Raman modes were assigned by comparison to other bismuth and titanate pyrochlores found in literature; $Bi_2Ti_2O_7$ displays evidence of displacive disorder in both the A and B site. A normally IR-active F_{1u} mode is assigned in the Raman spectra at low frequencies, possibly due to the displacement of the Bi atom from its ideal position via a relaxation of the selection rules. Additionally, evidence of displacement in the Ti atomic position is provided by the atypical spectroscopic behavior of the Ti−O modes at the higher range of the Raman spectra. The IR spectra were fit to an oscillator model from which the real and imaginary parts of the dielectric function were obtained. The low-frequency O−A−O and O′−A−O′ phonon modes are pushed to lower frequencies due to the large mass of the Bi ion. The appearance of the ω_n^b also indicates a disorder of the A site and O′ displacement.

dx.doi.org/10.1021/jp5095883 | J. Phys. Chem. C 2014, 118, 28797−28803

AUTHOR INFORMATION

Corresponding Author

*E-mail: chris114@ufl.edu.

Notes

The authors declare no competing financial interest.

ACKNOWLEDGMENTS

This work is supported by the U.S. National Science Foundation under grant DMR 0449710. The authors thank Robert Kasse for assistance with the Raman measurements.

REFERENCES

(1) Banys, J.; Ivanov, M.; Rudys, S.; Li, J.; Wang, H. Dielectric Properties of Cubic Bismuth Based Pyrochlores Containing Lithium and Fluorine. *J. Eur. Ceram. Soc.* **2010**, *30*, 385−388.

(2) Cann, D. P.; Randall, C. A.; Shrout, T. R. Investigation of the Dielectric Properties of Bismuth Pyrochlores. *Solid State Commun.* **1996**, *100*, 529−534.

(3) Du, H. L.; Yao, X.; Wang, H. Relaxor-like Behavior of Bismuth-Based Pyrochlores Containing Sn. *J. Electroceram.* **2008**, *21*, 222−225.

(4) Kamba, S.; Porokhonskyy, V.; Pashkin, A.; Bovtun, V.; Petzelt, J.; Nino, J. C.; Trolier-McKinstry, S.; Lanagan, M. T.; Randall, C. A. Anomalous Broad Dielectric Relaxation in $Bi_{1.5}Zn_{1.0}Nb_{1.5}O_7$ Pyrochlore. *Phys. Rev. B* **2002**, *66*, 054106.

(5) Liu, Y.; Withers, R. L.; Nguyen, H. B.; Elliott, K.; Ren, Q.; Chen, Z. Displacive Disorder and Dielectric Relaxation in the Stoichiometric Bismuth-Containing Pyrochlores, $Bi_2MIIINbO_7$ (M = In and Sc). *J. Solid State Chem.* **2009**, *182*, 2748−2755.

(6) Lufaso, M. W.; Vanderah, T. A.; Pazos, I. M.; Levin, I.; Roth, R. S.; Nino, J. C.; Provenzano, V.; Schenck, P. K. Phase Formation, Crystal Chemistry, and Properties in the System Bi_2O_3−Fe_2O_3−Nb_2O_5. *J. Solid State Chem.* **2006**, *179*, 3900−3910.

(7) Nino, J. C.; Lanagan, M. T.; Randall, C. A. Dielectric Relaxation in Bi_2O_3−ZnO−Nb_2O_5 Cubic Pyrochlore. *J. Appl. Phys.* **2001**, *89*, 4512−4516.

(8) Valant, M. Dielectric Relaxations in Bi_2O_3−Nb_2O_5−NiO Cubic Pyrochlores. *J. Am. Ceram. Soc.* **2009**, *92*, 955−958.

(9) Vanderah, T. A.; Guzman, J.; Nino, J. C.; Roth, R. S. Stability Phase-Fields and Pyrochlore Formation in Sections of the Bi_2O_3−Al_2O_3−Fe_2O_3−Nb_2O_5 System. *J. Am. Ceram. Soc.* **2008**, *91*, 3659−3662.

(10) Esquivel-Elizondo, J. R.; Hinojosa, B. B.; Nino, J. C. $Bi_2Ti_2O_7$: It Is Not What You Have Read. *Chem. Mater.* **2011**, *23*, 4965−4974.

(11) Levin, I.; Amos, T. G.; Nino, J. C.; Vanderah, T. A.; Randall, C. A.; Lanagan, M. T. Structural Study of an Unusual Cubic Pyrochlore $Bi_{1.5}Zn_{0.92}Nb_{1.5}O_{6.92}$. *J. Solid State Chem.* **2002**, *168*, 69−75.

(12) Turner, C. G. Dielectric Phenomena of Oxides with Fluorite Related Super Structures. Ph.D. Thesis, University of Florida, Gainesville, FL.

(13) Nino, J. C.; Lanagan, M. T.; Randall, C. A. Phase Formation and Reactions in the Bi_2O_3−ZnO−Nb_2O_5−Ag Pyrochlore System. *J. Mater. Res.* **2001**, *16*, 1460−1464.

(14) Rousseau, D. L.; Bauman, R. P.; Porto, S. P. S. Normal Mode Determination in Crystals. *J. Raman Spectrosc.* **1981**, *10*, 253−290.

(15) Chen, M. H.; Tanner, D. B.; Nino, J. C. Infrared Study of the Phonon Modes in Bismuth Pyrochlores. *Phys. Rev. B* **2005**, *72*.

(16) Vandenborre, M. T.; Husson, E. J. Comparison of the Force Field in Various Pyrochlore Families. I. $A_2B_2O_7$ Oxides. *Solid State Chem.* **1983**, *50*, 362−71.

(17) Melot, B.; Rodriguez, E.; Proffen, T.; Hayward, M. A.; Seshadri, R. Displacive Disorder in Three High-k Bismuth Oxide Pyrochlores. *Mater. Res. Bull.* **2006**, *41*, 961−966.

(18) Arenas, D. J.; Gasparov, L. V.; Qiu, W.; Nino, J. C.; Patterson, C. H.; Tanner, D. B. Raman Study of Phonon Modes in Bismuth Pyrochlores. *Phys. Rev. B* **2010**, *82*, 214302. 18.

(19) Gupta, H. C.; Brown, S.; Rani, N.; Gohel, V. B. Lattice Dynamic Investigation of the Zone Center Wavenumbers of the Cubic $A_2Ti_2O_7$ Pyrochlores. *J. Raman Spectrosc.* **2001**, *32*, 41−44.

(20) Vandenborre, M. T.; Husson, E.; Chatry, J. P.; Michel, D. J. Rare-Earth Titanates and Stannates of Pyrochlore Structure; Vibrational Spectra and Force Fields. *Raman Spectrosc.* **1983**, *14*, 63−71.

(21) McCauley, R. A. Infrared Absorption Characteristics of the Pyrochlore Structure. *J. Opt. Soc. Am.* **1973**, *63*, 721−5.

(22) Saha, S.; Ghalsasi, P.; Muthu, D. V. S.; Singh, S.; Suryanarayanan, R.; Revcolevschi, A.; Sood, A. K. Phonon Anomalies and Structural Transition in Spin Ice $Dy_2Ti_2O_7$: A Simultaneous Pressure-Dependent and Temperature-Dependent Raman Study. *J. Raman Spectrosc.* **2012**, *43* (8), 1157−1165.

(23) Patterson, C. H. First-Principles Calculation of the Structure and Dielectric Properties of $Bi_2Ti_2O_7$. *Phys. Rev. B* **2010**, *82*.

(24) Hong, W.; Huiling, D.; Xi, Y. Structural Study of Bi_2O_3−ZnO−Nb_2O_5 Based Pyrochlores. *Mater. Sci. Eng., B* **2003**, *99*, 20−24.

(25) Lummen, T. T. A.; Handayani, I. P.; Donker, M. C.; Fausti, D.; Dhalenne, G.; Berthet, P.; Revcolevschi, A.; van Loosdrecht, P. H. M. Phonon and Crystal Field Excitations in Geometrically Frustrated Rare Earth Titanates. *Phys. Rev. B* **2008**, *77*.

(26) Saha, S.; Singh, S.; Dkhil, B.; Dhar, S.; Suryanarayanan, R.; Dhalenne, G.; Revcolevschi, A.; Sood, A. K. Temperature-Dependent Raman and X-ray Studies of the Spin-Ice Pyrochlore $Dy_2Ti_2O_7$ and Nonmagnetic Pyrochlore $Lu_2Ti_2O_7$. *Phys. Rev. B* **2008**, *78*, 214102/1−214102/10.

(27) Wooten, F. *Optical Properties of Solids*; Academic Press: New York, 1972.

(28) Henke, B. L.; Gullikson, E. M.; Davis, J. C. X-ray Interactions—Photoabsorption, Scattering, Transmission, and Reflection at E = 50−30,000 eV, Z = 1−92. *At. Data Nucl. Data Tables.* **1993**, *55*, 349.

(29) Kumar, S.; Gupta, H. C. First Principles Study of Zone Centre Phonons in Rare-Earth Pyrochlore Titanates, $RE_2Ti_2O_7$ (RE = Gd, Dy, Ho, Er, Lu, Y). *Vib. Spectrosc.* **2012**, *62*, 180−187.